4D PRINTING OF COMMERCIAL BASED CONDUCTIVE POLYLACTIC ACID: STRENGTH AND RESISTANCE PROPERTIES

A. Amram[1], M. Faigenblat[1], A. Ulanov[1], D. Richkov[1], M. Ayal[1], D. Ashkenazi[2,*], A. Stern[1,3]

[1] School of Mechanical Engineering, Afeka Academic College of Engineering, Tel Aviv, 6998812, Israel
[2] Tel Aviv University, Ramat Aviv 6997801, Israe; ORCID: 0000-0001-5871-1903
[3] Department of Materials Engineering, Ben-Gurion University of the Negev, Beer Sheva 8410501, Israel
* Corresponding author: danaa@tauex.tau.ac.il

ABSTRACT

Four-dimensional (4D) printing technology is an innovative concept integrating between the conventional 3D printing additive manufacturing (AM) and smart materials programed to change properties or shape over time in response to environmental stimuli. This study aims to characterize the strength and electrical resistance of a commercial electrically conductive polylactic acid (PLA) with carbon black (CB) particles printed by fused filament fabrication (FFF) technique to evaluate the development feasibility of two sensor prototypes: (1) a load-cell sensor, and (2) a temperature sensor. Experiments were performed to study the orientation and raster angle–dependent mechanical and electrical performance of a PLA-CB conductive polymer manufactured by AM-FFF technology. A good agreement was observed between the data received from the manufacturer and the experimental density of the conductive AM-FFF PLA-CB three-point bending samples. The mechanical properties of 3D-printed PLA-CB were characterized based on three-point bending flexural test. Two build orientations (flat and upright) and three raster patterns (0°/90°, +45°/-45°, and concentric) were printed to check the optimal mechanical properties for electrical conductivity; six samples were printed for each one of the six configuration. The three-point bending flexural test results of the examined 36 specimens demonstrated that the samples printed in the concentric and +45°/-45° raster patterns exhibit the best mechanical properties, with the highest flexural strength and flexural modulus of elasticity in the flat orientation. Nevertheless, the concentric pattern has an advantage over the +45°/-45° pattern due to higher density and homogeneity. To examine the electrical resistance of the PLA-CB material another 12 specimens were printed and divided into four groups, each with different lengths. The electrical intrinsic resistivity was calculated from the geometry of the specimens and the measured resistance, with an average value of 13.2 [Ω·cm]. To check the production feasibility of a load-cell sensor prototype the effect of load on electrical conductivity was examined, however no effect of load on resistance was discovered. To prove the production feasibility of a sensor prototype for temperature measurements a preliminary device was designed and the effect of increasing and decreasing the temperature between 24 and 42 ºC on electrical resistance was examined. Based on the experimental results a calibration function was built linking between the temperature and the material's resistance.

KEYWORDS: fused filament fabrication (FFF), conductive polymer composites, carbon black (CB), 4D printing, polylactic acid (PLA)

1. INTRODUCTION

The term additive manufacturing (AM) or 3D printing covers several manufacturing technologies that build parts layer-by-layer. The acceptance of AM has continuously increased in industry since its origin in the rapid prototyping field in the early 1980s. Technologies for attaining materials printing have continued to become less expensive and more accessible in various industrial applications beyond rapid prototyping. AM offers reliable, flexible, fast design, and cost-effective manufacturing techniques mainly because it does not need any special tooling and reduces material wastage. AM processes construct three-dimensional components by adding layers of materials on top of one another, allowing the fabrication of complex customized parts directly from computer-aided design (CAD) software without the use of additional tools or expensive processing stages [1-4].

Date of submission/acceptance: 11.08.2023/-

Fused filament fabrication (FFF) is an AM process based on a thermoplastic polymer filament fed into a liquefier and normally extruded through a circular nozzle at its melting temperature. The incoming solid filament acts as a piston to push and extrude the melted polymer through the nozzle to produce a thin two-dimensional layer on top of another, resulting in a three-dimensional product [1-5]. The structure and properties of the FFF products are expected to be anisotropic as the components are built in the Z direction by depositing relatively thin layers. During the thin layer deposition process (Fig. 1a to e), the molten polymer extruded from the nozzle is compressed between the nozzle and the previously existing layer (Fig. 2) [6]. Thus, it deforms plastically, and its cross-section becomes relatively oval (Fig. 1 and 2) [6]; this increases the contact area (wetting), leading to improved welding between the rasters (Fig. 2). The permanent bonding between two adjacent layers is formed by local thermal diffusion of neighboring rasters, as mentioned above (Fig. 2) [7]. The mechanical properties of FFF structures depend on the polymer material, structural discontinuities, geometry of the structure, and FFF parameters. The most common discontinuities affecting FFF printed parts mechanical properties are imperfect weld-lines (poor bonding between rasters) and intra-layer/inter-layer porosity [4-9]. The commonly used commercial polymers for AM-FFF are acrylonitrile butadiene styrene (ABS), polyamide (PA), and polylactic acid (PLA), where the PLA material combines consistency of printability with a relatively high strength and deformation to failure [10-16].

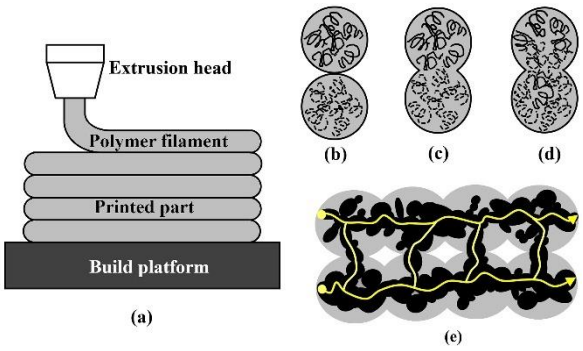

Fig. 1. Schemes of the bond formation during the FFF AM process: (a) the macroscopic building procedure of thin polymeric layers; (b) surface contacting at the microscopic level between two molten plastic extruded filament layers; (c) necking growth between two filament layers; (d) diffusion process at the interface between two layers; and (e) the microstructural nature of the conductive polymeric materials owing to the presence of conductive carbon black (CB) particles within the PLA filament, where the grey areas represents the PLA matrix, the black areas represents the CB particles, and the yellow line represents the electrical conductive path [6].

4D printing concept (Fig. 3), with the fourth dimension referring to time alteration, is basically a group of AM technologies that use smart metals, ceramics, and polymers that show the ability of creating structures whose shape, properties, or functionality can vary with time under different stimuli [17-21]. To control a 3D-printed structure and allow it to function after printing, materials should have unique characteristics that make them responsive to external stimuli. Among those unique programed materials, it is worth mentioning the 4D printed conductive polymers [22, 23]. Another kind of unique programed materials are the shape-memory polymers (SMPs) that have the ability to recover from an impermanent programmed form to a permanent one in response to an exterior stimulus [24].

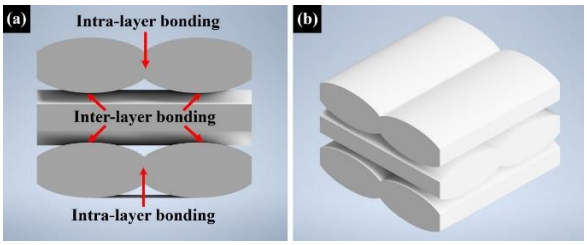

Fig. 2. Visualization of the PLA-BC raster 0°/90° building configuration unit cell (CAD model), showing the welding between the polymeric fibers located at the same layer (intra-layer weld), and the weld between two adjacent layers (inter-layer weld): (a) front view; and (b) isometric view [7].

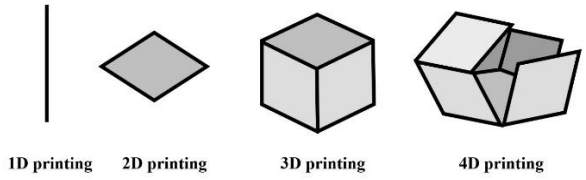

Fig. 3. The dimensions of AM technologies: A schematic illustration explaining the differences between one-dimensional (1D), two-dimensional (2D), three-dimensional (3D), and four-dimensional (4D) printing technologies, where the 4D printing integrates between 3D printing AM technologies and smart materials that are programed to change properties or shape with time [17].

Thermoplastic composites are widely used in different industries due to their light weight and good mechanical properties [25]. The conductive polymers present intrinsic electrical conductivity due to the incorporation of conductive agglomerates/particles within the polymeric matrix. The conductive polymeric filaments with carbon black (CB) as filler are the ones that aroused the most interest due to their being easy to operate [18]. Conductive CB types of filler are based on the thermal-oxidative decomposition process of hydrocarbons. The material exists in the form of

discrete particles, however, during the fabrication process of CB its spherical particles (primary particles) aggregate into chains or clusters (Fig. 1). The quantity of conductive particles needed to make a composite polymer conductive, in addition to the type of CB material, is influenced by the polymer type and properties, such as crystallinity, stability, surface tension, and viscosity. In recent studies the influence of different printing parameters on the resistivity [Ω·cm] of the PLA-CB composites was studied [26-29].

The microstructural arrangement and the amount and distribution of the conductive particles (i.e., CB particles) within the polymeric matrix determine the nature of the electrically conductive material [27-31]. When the conducting CB content is gradually increased, the polymer experiences an insulator-to-conductor transition. The classical percolation theory is employed to describe the electrically conducting behavior of composites consisting of insulating matrices and conducting fillers. The electrical conductivity of CB–polymer composite structure depends on the structure of the CB particles, however differs from the expectations of percolation theory [31].

The resistivity [Ω·cm] of the AM-FFF PLA-CB material depends on the rasters' bonding and formation of CB aggregates creating the electric paths within the composite polymer, see the schematic representation in Fig. 1b-e. These electric paths are established at dual levels [27]: (1) at the filament level the electric conduction is formed along the filament direction, and (2) at the inter-filament/inter-layer level, electric conduction is provided between different rasters/layers. These dissimilarities between the electric paths formed within and between the AM-FFF PLA-CB filaments determine the general resistivity of the printed polymer [27].

The CB conductive particles within the printed AM-FFF PLA-CB rasters can be presumed to be distributed homogeneously. A rather constant resistivity can be expected along the filament orientation, as the electric resistance [Ω] of the composite polymer depends directly on the conductive paths formed by CB particles (Fig. 1e). The overall resistance of the AM-FFF PLA-CB specimens should be significantly influenced by the AM printing strategy and the subsequent bonding developed between rasters. For example, in longitudinal specimens the electric current follows conductive paths created within the raster's printing direction. In this type of specimen, a relatively low resistivity is expected and hence the creation of conductive paths through filaments bonding is less significant. Yet, if the printing direction is extremely misaligned with the conduction direction (as in the +45º/-45º specimens), the conductive paths created in between the rasters are becoming increasingly involved in the charge conduction process, thus leading to a higher resistivity [27].

The AM-FFF PLA-CB manufacturing parameters play a double role: (a) the printing conditions effect the mesostructured of the composite polymer, as they rule the bonding process that determine the inter-filament porosity, (b) the volume optimization of CB fraction to ensure the dielectric transition to conductor, nonetheless not too high to lead to blocked nozzles and brittle filaments. The distribution of the conductive CB particles within the PLA matrix determines the possible pathways for charge conduction, and a good bonding is essential to allow for a decent PLA-CB conductivity [27].

The mechanical properties of the AM-FFF PLA matrix and the CB content determine the microstructural features of the conductive composite material, as well as its strength, stiffness, and ductility [27]. Increasing the CB content inside the matrix improves the conductivity of the composite polymer, yet, at the same time it reduces the final strength of the product [29]. When the CB conductive particles are filled within the PLA matrix, the bonding process is negatively affected, leading to a poorer contact zone and lower wetting between filaments resulting in a significant increase of porosity. This behavior can be explained by a limitation in polymeric PLA chains' mobility according to the existence of the CB filler particles (Fig. 1b-c). The electrical conduction value depends on the continuation of physical pathways of the CB conductive particles [27]. Hence, the general behavior of AM-FFF conductive polymers should account for both electrical and mechanical performances since the local deformation of the polymeric matrix may affect the relative position of the conductive CB particles, consequently significantly changing the material resistivity [31-37]. Conductive composites with polymeric matrix have been labelled as promising materials for various applications, such as energy storage, flexible electronics, sensors, bioelectronic devices [27, 37] etc.

In the present study, as a part of an on-going project dealing with the properties of AM-FFF printed polymer specimens [6, 7, 38-42], an effort has been made to advance the knowledge on mechanical and electrical properties of a commercial conductive PLA material with CB particles used for applications in the field of 4D printing.

2. EXPERIMENTAL

2.1. Conductive PLA Material and AM-FFF Specimens Fabrication

In this research, two types of samples were 3D-printed by the FFF technology in order to characterize the strength and resistance of an electrically conductive AM material for two kinds of sensor application: (1) a load-cell sensor, and (2) a temperature sensor. For this purpose, a commercial electrically conductive composite PLA-CB filament (Protopasta Co., Ltd) was used. The basic properties of this material and printing parameters as recommended by the manufacturer are presented in Table 1.

Table 1. The 3D printing parameters and properties of the electrically conductive composite PLA-CB filament (with PLA as base material and CB as additive particles), as recommended by the manufacturer (Protopasta Co., Ltd).

Parameter	Recommended value
Density [g/cm^3]	1.24
Filament diameter [mm]	1.75
Melting point [°C]	155
Electrical intrinsic resistivity in the Z direction [Ω·cm]	30
Electrical intrinsic resistivity in the X and Y directions [Ω·cm]	115
Printed speed [mm/s]	25–45
Nozzle temperature [°C]	215
Heated bed temperature [°C]	60

The main 3D printing parameters of the FFF printer that were used to print the current PLA-CP samples are summarized in Table 2.

Table 2. The current used 3D printing parameters that were used in order to print all examined AM-FFF PLA-CB samples.

Parameter	Recommended value
Layer height [mm]	0.2
Wall thickness [mm]	0.4
Top and bottom thickness [mm]	0
Infill density [%]	99
Infill pattern	Concentric/lines
Printing temperature [°C]	230–235
Build temperature [°C]	50–60
Print speed [mm/s]	30
Travel speed [mm/s]	150

2.2. The Three-point Bending Specimens and Mechanical Testing

Eighteen three-point bending specimens were printed with a Creality CR-10 Smart Pro AM-FFF 3D printer and another eighteen three-point bending specimens were printed with a Creality Ender-3 Pro 3D printer. The build orientation and printing parameters are shown in Fig. 4 and Table 2, respectively. The beam-shaped specimens were manufactured according to ASTM D790 standard for three-point bending flexural test and their dimensions were 127 [mm] × 12.7 [mm] × 3.2 [mm] (Fig. 4a). The ASTM D790 standard is commonly used to determine the flexural properties of unreinforced and reinforced plastics and electrical insulating materials.

The specimens were produced with filament made of PLA-CB composite thermoplastic material. The configuration was described by two orthogonal orientation notations (flat and upright) (Fig. 4b), whereas for each orientation three raster patterns (0°/90°, +45º/-45º, and concentric) were 3D-printed (Fig. 4 and Table 3).

The printing time of each group of samples varied between 54 and 82 [min] for the flat and the upright orientations, respectively. Dimensions and density were measured and calculated for each specimen prior to the bending test.

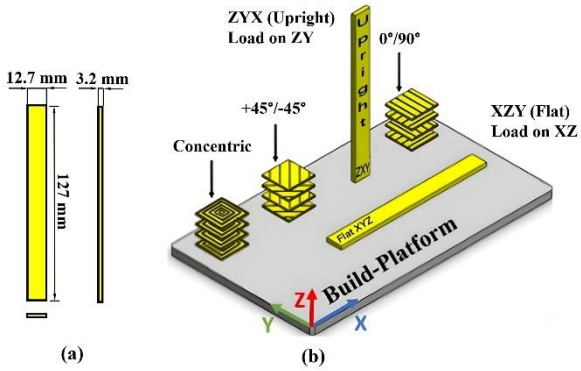

Fig. 4. The AM-FFF PLA-CB three-point bend test specimens: a) front, side and top views; b) an isometric SolidWorks CAD model of the 3D-printed specimens, showing the six print strategy configurations [6]: flat 0°/90°, flat +45º/-45º, on-edge 0°/90°, on-edge +45º/-45º, upright 0°/90°, and upright +45º/-45º specimens.

Table 3. Description of the experimental three-point bending specimens, summarizing the number of printed specimens from each combination of raster patterns and build orientations.

Build orientation	Raster pattern	Number of printed specimens
Flat	0°/90°	6
Flat	+45º/-45º	6
Flat	Concentric	6
Upright	0°/90°	6
Upright	+45º/-45º	6
Upright	Concentric	6

The three-point bending flexural test of the AM-FFF PLA-CB samples was conducted on a computerized MTS© E43-504 universal testing machine equipped with a three-point bend fixture and a deflection gage (Fig. 5). The data was used to calculate the flexural modulus of elasticity [GPa] and the flexural strength [MPa]. The experimental flexural strength, $\sigma_{b\ (max)}$, was calculated using the formula: $\sigma_{b\ (max)} = \frac{3 \cdot F \cdot L}{2 \cdot b \cdot h^2}$ where F [N] is the maximum applied load at the fracture point, L [mm] is the distance between the two anvils, and b [mm] and h [mm] are the dimensions of the specimen's cross-section width and thickness, respectively. The experimental modulus of

elasticity, E, was calculated using the formula: $E = \frac{L^3 \cdot F}{4 \cdot b \cdot h^3 \cdot \delta}$ where δ [mm] is the beam deflection.

Fig. 5. The MTS© E43-504 universal testing machine system, equipped with a bend fixture; and AM-FFF PLA-CB bend test specimen during performance of a three-point bend test.

2.3. Conductive PLA-CB Specimens' Description, Electrical Resistance Measurements and Resistivity Calculations

Based on the tested mechanical properties, the flat building orientation combined with the concentric pattern (flat-concentric printing configuration strategy) were selected to build the specimens used for resistivity measurements. The geometry of the AM-FFF PLA-CB resistance specimen is shown in Fig. 6. The measured dimensions of the sample were (14.5 + x) [mm] × 8 [mm] × 6 [mm]. Fifteen samples were printed using a Creality CR-10 Smart Pro AM-FFF 3D printer. The printed specimens were divided into four groups (A-D, Table 4) according to their different distance, x, between holes (50, 100, 150, and 200 [mm], Fig. 6a). The 3D printing parameters of the AM-FFF PLA-CB samples designed for electrical resistance measurements are shown in Table 2. The printing time of each group of samples varied between 34 and 71 [min].

The electrical intrinsic resistivity [Ω·cm] of the samples was calculated using the formula: $\rho = R \cdot \frac{A}{l}$ where R [Ω] is the resistance of the specimen, A [mm^2] is the cross-section of the specimen, and l [mm] is the length of the specimen.

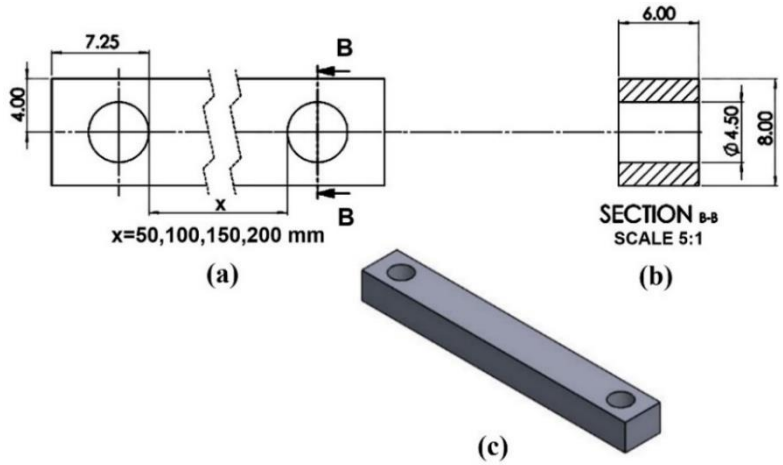

Fig. 6. The CAD model geometry of the PLA-CB resistance specimen: a) upper view; b) side view; c) isometric view (designed with SolidWorks 2022)

Table 4. The description of the examined AM-FFF PLA-CB resistance specimens (A-D) according to their different distance, x, between the two holes (x = 50, 100, 150, and 200 [mm])

Group no.	Build orientation	Raster pattern	Distance between holes [mm]	Number of printed specimens
A	Flat	Concentric	50	6
B	Flat	Concentric	100	3
C	Flat	Concentric	150	3
D	Flat	Concentric	200	3

2.4. The Influence of the Applied Load on the Electrical Resistance Values of AM-FFF PLA-CB Specimens

AM-FFF PLA-CB samples were designed to measure the change of the electrical resistance as a function of the applied load (Fig. 7) and were 3D-printed according to the parameters presented in Table 2. Nine samples were 3D-printed using the Creality Ender-3 Pro 3D printer AM-FFF instrument according to the

flat-concentric printing configuration strategy. The printing time of these samples was 141 [min].

The tests were performed with the MTS© E43-504 universal testing machine (Fig. 8), according to the ASTM D695 standard and the electrical resistance was measured by the Fluke 287 electronics multi-meter instrument. No changes were detected in the electrical resistance of all nine tested samples as a function of the applied load.

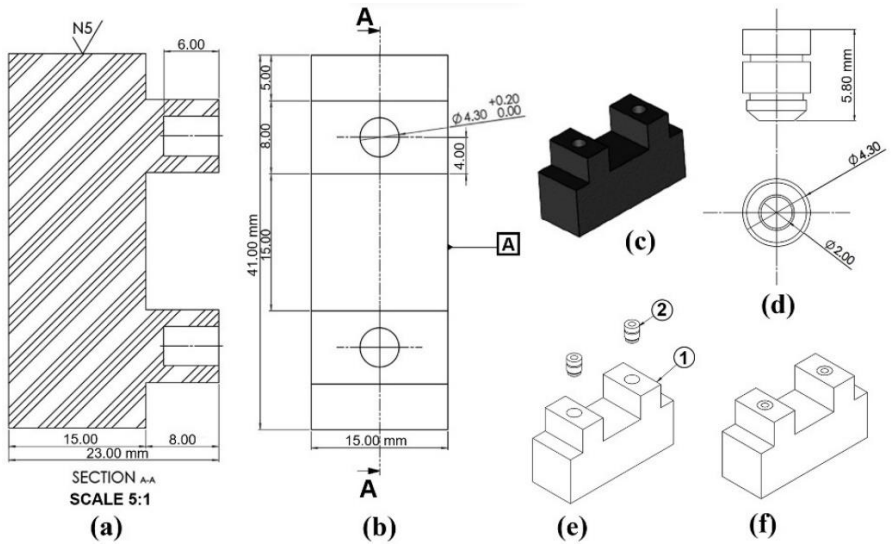

Fig. 7. The CAD model geometry of the PLA-CB specimen designed for measuring the electrical resistance as a function of the applied load: a) front view; b) upper view; and c) isometric view; d) the brass insert; e)-f) isometric view of the specimen with the brass insert (designed with SolidWorks 2022)

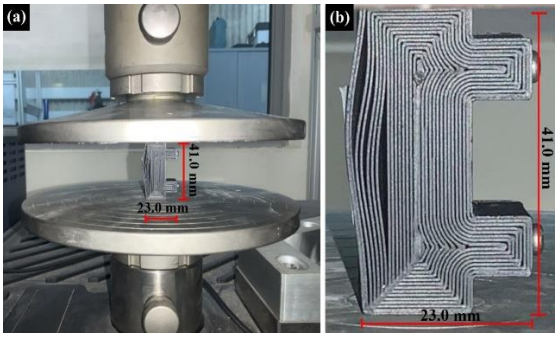

Fig. 8. The experimental system: a) the MTS© E43-504 universal testing machine equipped with a load cell and an AM-FFF PLA-CB test specimen; b) higher magnification of the test specimen at failure (flat-concentric printing configuration).

2.5. Resistance Measurements of the AM-FFF PLA-CB Material as a Function of the Temperature Variation

Twelve PLA-CB samples were designed (Fig. 9) and 3D-printed using the Creality Ender-3 Pro 3D printer AM-FFF instrument according to the parameters presented in Table 2 to measure the electrical resistance as a function of the temperature. The samples were printed according to the flat-concentric printing configuration strategy. The printing time of these samples was between 47 and 50 [min]. The electrical resistance was measured by the Fluke 287 electronics multi-meter instrument. The printed specimens were divided into four groups (Table 5) according to their central surface thickness (Fig. 9a).

Table 5. The description of the examined AM-FFF PLA-CB resistance specimens (1-4) (Fig. 9a, where x = 0, 0.5, 1, 1.5 [mm] is the additional thickness of the central area)

Group no.	Build orientation	Raster pattern	Total thickness [mm]	Number of printed specimens
1	Flat	Concentric	0.4	3
2	Flat	Concentric	0.9	3
3	Flat	Concentric	1.4	3
4	Flat	Concentric	1.9	3

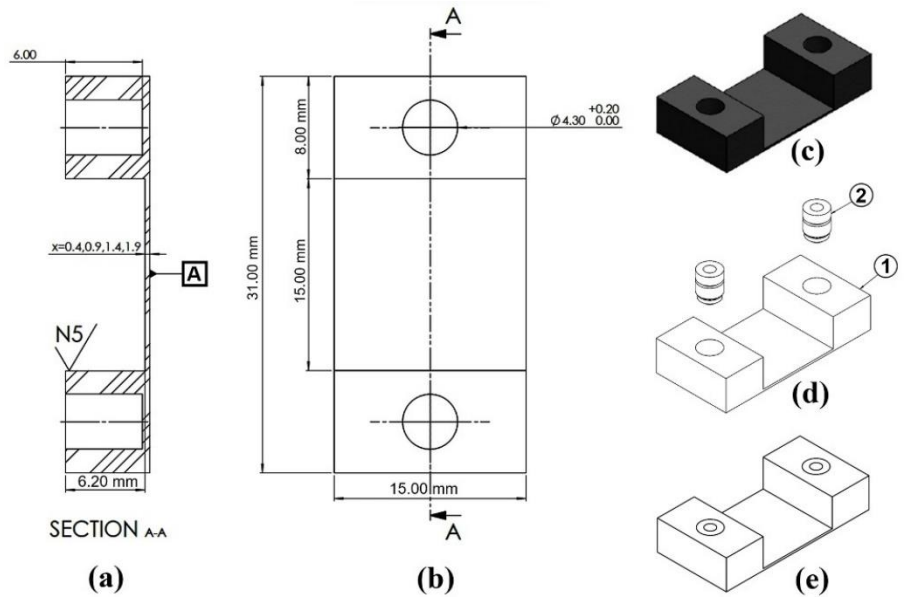

Fig. 9. The CAD model geometry of the PLA-CB specimen designed for measuring the electrical resistance as a function of the temperature variation: a) front view; b) upper view; c) isometric view, d)-e) isometric view of the specimen with the brass insert (designed with SolidWorks 2022)

The electrical resistance as a function of the temperature was measured for four different thicknesses of the samples' central surface (Fig. 9a).

In order to measure the temperature values, the samples were glued with thermal glue to a piece of aluminum and placed inside a heated pool of water, and then the resistance was measured up (increased temperature) and down (decreased temperature) in a temperature range of 24 and 42 °C.

3. RESULTS

3.1. Density Measurements

The density results of the AM-FFF PLA-CB three-point bending samples are presented in Table 6. The average density values of the flat configuration were between 0.94±0.11 [gr/cm^3] (for the 0°/90° pattern) and 1.17±0.07 [gr/cm^3] (for the concentric pattern). The average density values of the upright configuration were between 1.00±0.07 [gr/cm^3] (for the 0°/90° pattern) and 1.20±0.08 [gr/cm^3] (for the concentric pattern) (Table 6). For these three-point bending samples, the higest density values were obtained for the upright-concentric. A good agreement was obtained between the measured experimental density of the 3D-printed three-point bending samples and the published data received from the manufacturer.

The density values of the AM-FFF PLA-CB electrical resistance specimens (A-D) are presnted in Table 7 for the flat-concentric printing configuration strategy, where the distance between the two holes was 50, 100, 150, and 200 for [mm] for specimens A, B, C, D, correspondingly. The uniformity of the density results for these resistance test specimens (Table 7), with density values between 1.18 and 1.19 [gr/cm^3], indicates a good printing quality.

3.2. Mechanical Properties

The maximal axial deflection values of the AM-FFF PLA-CB three-point bending samples for the different printing configurations are presented in Table 8. The results reveal that the largest deflection values exist in the flat-concentric and flat with +45º/-45º printing configurations (Table 8).

The flexural strength values obtained from the three-point bending flexural test values, $\sigma_{b\,(max)}$, of the AM-FFF PLA-CB specimens are presented in Table 9. The results revealed that the largest flexural strength values exist in the flat-concentric and flat with +45º/-45º printing configurations (Table 9), with values of 46.33 [MPa] for the flat with +45º/-45º printing configuration and 45.30 [MPa] for the flat-concentric printing configuration (Table 9). For a comparison, the flexural strength value published in the literature is 30.8 [MPa] [27]. The difference between the published flexural strength [27] and the current experimental results can be explained according to the use of dissimilar printing configuration strategy (different printing directions and densities).

The flexural modulus of elasticity values received from the three-point bend tests of the AM-FFF PLA-CB specimens (samples 4-6) for the flat and upright build orientations and 0°/90°, +45º/-45º, and concentric raster patterns are presented in Table 10. The current results reveal that the largest flexural modulus of elasticity values exist in the flat with +45º/-45º and flat-concentric printing configurations, with values of 1.84 [GPa] and 1.68 [GPa], respectively (Table 10). For a comparison, the flexural modulus of

elasticity value published in the literature is 0.68 [GPa] [27]. The difference between the published flexural modulus of elasticity [27] and the current experimental results can be explained according to the use of different printing configuration strategies (different printing directions and densities).

Table 6. The measured density values of the AM-FFF PLA-CB three-point bending samples for the flat and upright build orientations and 0°/90°, +45º/-45º, and concentric raster patterns

Density [gr/cm^3]						
Sample no.	**Flat**			**Upright**		
	+45°/-45°	**0°/90°**	**Concentric**	**+45°/-45°**	**0°/90°**	**Concentric**
1	1.10	1.10	1.13	1.08	0.97	1.11
2	1.12	1.10	1.12	1.09	1.01	1.12
3	1.12	1.08	1.13	1.12	0.95	1.12
4	1.27	0.96	1.17	1.17	0.76	1.15
5	1.28	0.92	1.21	1.27	0.97	1.17
6	1.27	0.95	1.22	1.26	0.84	1.15
Average Density	1.13±0.02	0.94±0.11	1.17±0.07	1.15±0.05	1.00±0.07	1.20±0.08

Table 7. The measured density values of the AM-FFF PLA-CB resistance specimens 50, 100, 150, and 200 [mm] (A-D) for the flat-concentric printing configuration strategy

Density [gr/cm^3]				
Measurement/ Group no.	**A**	**B**	**C**	**D**
1	1.20	1.21	1.18	1.20
2	1.19	1.15	1.18	1.16
3	1.16	1.19	1.19	1.20
Average value	1.18	1.18	1.19	1.19

Table 8. The deflection values received from the three-point bend flexural tests of the AM-FFF PLA-CB three-point bending specimens of the flat and upright build orientations and 0°/90°, +45º/-45º, and concentric raster patterns. Samples 1-3 were printed with the Creality CR-10 Smart Pro 3D printer and samples 4-6 were printed with the Creality Ender-3 Pro 3D printer, respectively

Deflection [mm]						
Sample no.	**Flat**			**Upright**		
	+45°/-45°	**0°/90°**	**Concentric**	**+45°/-45°**	**0°/90°**	**Concentric**
1	1.00	1.20	1.20	0.25	0.60	0.45
2	1.50	1.10	1.80	0.30	N.A.	0.50
3	1.10	1.20	1.15	0.20	0.10	0.40
Average value of samples 1-3	1.20	1.17	1.38	0.25	0.35	0.45
4	1.70	1.30	2.30	1.20	N.A.	0.70
5	2.30	1.00	2.00	0.50	0.20	0.85
6	2.00	1.20	2.00	0.85	0.05	0.80
Average value of samples 4-6	2.00	1.17	2.00	0.85	0.13	0.78

Table 9. The flexural strength values, $\sigma_{b\,(max)}$, received from the three-point bend tests of the AM-FFF PLA-CB specimens (samples 4-6), for the flat and upright build orientations, and 0°/90°, +45°/-45°, and concentric raster patterns

Flexural strength $\sigma_{b\,(max)}$ [MPa]						
Sample no.	**Flat**			**Upright**		
	+45°/-45°	**0°/90°**	**Concentric**	**+45°/-45°**	**0°/90°**	**Concentric**
4	44.23	9.70	43.46	12.47	N.A.	12.32
5	46.00	8.61	46.03	9.85	2.12	13.59

6	46.65	10.63	46.41	17.26	0.24	13.57
Average value	46.33	9.64	45.30	13.19	1.18	13.57

Table 10. The flexural modulus of elasticity values, E, received from the three-point bend tests of the AM-FFF PLA-CB specimens (samples 4-6) of the flat and upright build orientations and 0°/90°, +45°/-45°, and concentric raster patterns

Flexural modulus of elasticity [GPa]						
Sample no.	**Flat**			**Upright**		
	+45°/-45°	**0°/90°**	**Concentric**	**+45°/-45°**	**0°/90°**	**Concentric**
4	2.15	0.63	1.59	0.87	N.A.	1.48
5	1.68	0.73	1.91	1.67	0.90	1.34
6	1.68	0.75	1.56	1.66	0.41	1.54
Average value	1.84	0.70	1.68	1.40	0.66	1.45

3.4. Electrical Resistance and Resistivity Values as a Function of the Temperature

The measured room-temperature electrical resistance [Ω] values of the AM-FFF PLA-CB specimens (for groups A-D according to their different samples' distance, x, between holes) are presented in Table 11. The calculated room-temperature electrical resistivity [Ω·cm] values of specimens A-D based on Table 11 are given in Table 12, with average value of 13.20 [Ω·cm], where the resistivity was calculated from the resistance and geometry of the specimens. The average resistivity values of specimens B, C and D are almost identical and varies between 12.53 [Ω·cm] for specimen C and 12.82 [Ω·cm] for specimen B, with values similar to the resistivity published by the manufacturer, yet, the average resistivity of sample type A is significantly larger (14.86 [Ω·cm]) (Table 12).

The electrical resistance values were measured as a function of the increased and decreased temperature for different additional central area thickness values, x = 0.5, 1, 1.5 [mm] (Table 13); linear calibration functions were built, linking between the temperature [^{o}C] and the resistance [Ω]. For example, the resistance calibration functions for increased temperature values and x=0.5, 1.0, and 1.5 [mm] can be described linearly as R=9.0773T+44.7 [Ω], R=8.1363T-8.99 [Ω], and R=5.7866T-0.9 [Ω], respectively. The electrical resistance values achieved for different increased and decreased temperatures are presented in Fig. 10 for specimens with different cross-sections. As expected, the results revealed that the resistance values increase when the temperature values increase. The results also show that when the central area increases the resistance decreases (Fig. 10).

The electrical resistance values were measured as a function of the increased and decreased temperature for different additional central area thickness values, x = 0.5, 1, 1.5 [mm] (Table 13); linear calibration functions were built, linking between the temperature [^{o}C] and the resistance [Ω]. For example, the resistance calibration functions for increased temperature values and x=0.5, 1.0, and 1.5 [mm] can be described linearly as R=9.0773T+44.7 [Ω], R=8.1363T-8.99 [Ω], and R=5.7866T-0.9 [Ω], respectively. The electrical resistance values achieved for different increased and decreased temperatures are presented in Fig. 10 for specimens with different cross-sections. As expected, the results revealed that the resistance values increase when the temperature values increase. The results also show that when the central area increases the resistance decreases (Fig. 10).

Table 11. The electrical resistance values of the AM-FFF PLA-CB A-D specimens that were measured for different distance, x, between holes (50, 100, 150, and 200 [mm], respectively). The measurements were done with RCL meter instrument designed for electrical resistant measurements (with basic instrument accuracy of 0.1%)

Resistance [Ω]				
Measurement/ Group no.	**A**	**B**	**C**	**D**
1	156.41	271.53	391.52	536.37
2	166.48	267.17	396.56	N.A.
3	163.52	274.00	394.23	N.A.
Average value	162.14	270.98	394.23	536.37

Table 12. The calculated electrical intrinsic resistivity values of the AM-FFF PLA-CB A-D specimens for different distance between holes (50, 100, 150, and 200 [mm], respectively)

Resistivity [Ω·cm]				
Measurement/ Group no.	**A**	**B**	**C**	**D**
1	14.51	12.76	12.42	12.71
2	15.26	12.80	12.76	N.A.
3	14.81	12.91	12.43	N.A.
Average value	14.86	12.82	12.53	12.71

Table 13. Electrical resistance values as a function of incensement and decrement of the temperature values for different central area thickness (Fig. 9a, x = 0, 0.5, 1, 1.5 [mm])

Increased temperature				Decreased temperature			
X [mm]	**0.5**	**1.0**	**1.5**	**X [mm]**	**0.5**	**1.0**	**1.5**
Temperature [°C]	**Resistance [Ω]**			**Temperature [°C]**	**Resistance [Ω]**		
24	260	196	145	42	423	306	250
26	280	200	149	40	412	293	241
28	298	214	158	38	388	275	228
30	319	229	168	36	360	255	217
32	339	246	180	34	340	236	200
34	353	267	197	32	325	225	188
36	373	288	210	30	310	213	178
38	393	307	222	28	295	204	171
40	411	319	233	26	282	193	163
42	419	328	240	24	270	172	153

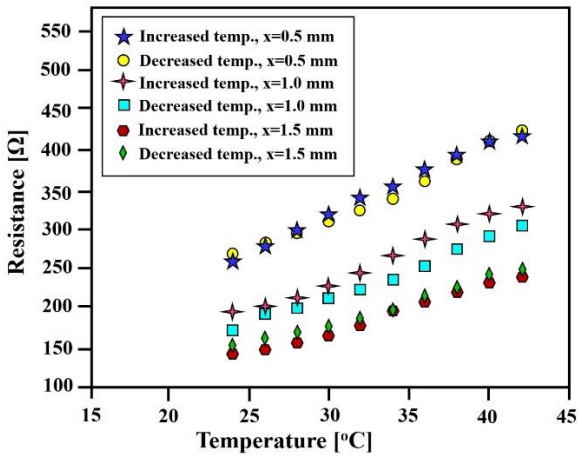

Fig. 10. Electrical resistance values vs. the temperature increased and decreased values for different central area thicknesses (Fig. 9a, x = 0, 0.5, 1, 1.5 [mm]). Each point in the graph is an average of three measurements

4. DISCUSSION

Four-dimensional printing is an emerging technological approach integrating between 3D printing AM and unique materials that can be programed to change their properties or shape through time in response to environmental stimuli [19-37]. This aims of this research were to characterize the mechanical and electrical properties of commercial electrically conductive AM-FFF PLA-CB specimens to demonstrate the feasibility of producing 4D printing load-cell and temperature sensors. In order to fulfil these goals, the mechanical properties of AM-FFF PLA-CB specimens were printed and tested, using six groups of different 3D printing configurations, composed of flat and upright build orientations combined with three raster patterns (0°/90°, +45°/-45°, and concentric). For each of the six groups of specimens, six samples were printed and examined by three-point bending flexural test in order to determine the most effective printing strategy (Table 3).

The obtained results show that there are clear differences between the properties achieved in the six dissimilar 3D printing configurations. The three-point bending flexural test results of the examined 36 specimens demonstrated that the samples printed in the concentric and +45°/-45° raster patterns exhibited the best mechanical properties of highest flexural strength and highest flexural modulus of elasticity in the flat build orientation. However, the concentric pattern had an advantage over the +45°/-45° pattern due to its higher density and homogeneity. Since the goal was to design a thermometer, the concentric filling shape was chosen to measure the electrical resistance and resistivity.

A good agreement was obtained between the published data received from the manufacturer and the current experimental density of the AM-FFF PLA-CB three-point bending samples (Table 1 and Table 6, respectively). The uniformity of the density results of the flat-concentric test specimens (Tables 6, 7) indicates a good printing quality.

The AM-FFF PLA-CB three-point bending test results revealed that the largest deflection values occur in the flat-concentric and flat with +45°/-45° printing configurations (Table 8). The three-point bend test

results of the AM-FFF PLA-CB specimens revealed that the largest flexural strength values exist in the flat-concentric and flat with +45º/-45º printing configurations, with values of 46.33 [MPa] and 45.30 [MPa] for the flat with +45º/-45º and flat-concentric printing configurations, respectively (Table 9), whereas the flexural strength value published by Carmona and Ravier (2002) is 30.8 [MPa]. The differences between the published flexural strength [30] and the current experimental AM-FFF PLA-CB flexural strength values (Table 9) result from the use of dissimilar printing configuration strategy.

The current AM-FFF PLA-CB flexural modulus of elasticity results had the largest values in the flat with +45º/-45º and flat-concentric printing configurations, with values of 1.84 [GPa] and 1.68 [GPa], respectively (Table 10), whereas the flexural modulus of elasticity value published in the literature is 0.68 [GPa] [28]. The difference between the published flexural modulus of elasticity [30] and the current experimental results can be explained according to the use of different printing configuration strategy (different printing directions and densities). Compared to regular PLA polymer, the addition of carbon black particles to the PLA matrix reduces the mechanical properties of the final printed specimens.

The room-temperature electrical intrinsic resistivity value of examined AM-FFF PLA-CB specimens is 13.2 [Ω·cm], where the average resistivity values of specimens B, C and D are almost identical, with values varied between 12.53 and 12.82 [Ω·cm] (for specimens C and B, respectively); these obtained values are near to the resistivity value published by the manufacturer. However, the average resistivity of specimen A is 14.86 [Ω·cm], which is notably larger than the value published by the manufacturer (Table 12).

The measured electrical resistance values of the AM-FFF PLA-CB specimens were decreased when the central area was increased according to larger specimens' cross-section (Fig. 10). The electrical resistivity values of the AM-FFF PLA-CB specimens were increased when the temperature values raised (Table 12). The results also show that when the thickness of the central area increased the resistance values were decreased (Fig. 10). The electrical resistivity was consistent in all the different specimens' length, which is with good agreement with the theory, but the current obtained resistivity values of the AM-FFF PLA-CB specimens are much higher than the electrical resistivity values of conductive metals, therefore, it is more challenging to use this AM-FFF PLA-CB material in applications of electric circuits.

5. SUMMARY AND CONCLUSIONS

Improved processing techniques were developed for 4D printing of PLA-CB (Protopasta Co., Ltd) conductive polymer allowing the building of sensors to be used for temperature measurements. The mechanical properties of 3D-printed PLA-CB were characterized by the three-point bending flexural test. Two build orientations (flat and upright) and three raster patterns (0°/90°, +45°/-45°, and concentric) were printed to check optimal mechanical properties for electrical conductivity measurements. The three-point bending flexural test results demonstrated that the best mechanical properties were achieved for specimens printed in the +45°/-45° and concentric raster patterns, with the highest flexural strength and flexural modulus of elasticity in the flat build orientation. Nevertheless, the concentric pattern offers better solution than the +45°/-45° pattern for the case of the temperature sensor due to its higher density and homogeneity. The reproducibility of the electrical resistance of the PLA-CB specimens was tested by measuring samples having different lengths. The electrical resistivity was calculated and an average value of 13.2 [Ω·cm] was attained. To check the production feasibility of a load-cell sensor prototype, the effect of load on electrical conductivity was examined, however no effect of load on resistance was discovered. To prove the production feasibility of the prototype device for temperature measurements, a preliminary sensor was designed and the effect of increasing and decreasing the temperature between 24 and 42 ºC on electrical resistance was examined. Based on the experimental results a calibration function was built linking between the temperature and the material's electrical resistance. The present study demonstrates the great potential of 4D printing technologies for sensor fabrication and strategies. The current improved processing techniques could lead to new applications for conductive polymers in advanced/complex areas such as medical devices and wearable electronics. For example, the research can lead to development of new types of digital thermometers to be included in medical devices such as splints for monitoring the healing process.

ACKNOWLEDGEMENTS

The research was supported by the Afeka Academic College of Engineering, to whom the authors are grateful. Thanks also go to V. Palei and S. Maman from the Afeka Academic College of Engineering, for their great engineering assistance and technical support.

REFERENCES

[1] **Penumakala, P. K., Santo, J., Thomas, A.**, *A critical review on the fused deposition modeling of thermoplastic polymer composites*, Composites Part B: Engineering, vol. 201, 2020, p. 108336, https://doi.org/10.1016/j.compositesb.2020.108336.

[2] **Goh, G. D., Yap, Y. L., Tan, H. K. J., Sing, S. L., Goh, G. L., Yeong, W. Y.**, *Process–structure–properties in polymer additive manufacturing via material extrusion: A review*, Critical Reviews in Solid State and Materials Sciences, vol. 45, iss. 2, 2020, pp. 113–133, https://doi.org/10.1080/10408436.2018.1549977.

[3] **Wickramasinghe, S., Do, T., Tran, P.**, *FDM-based 3D printing of polymer and associated composite: A review on mechanical properties, defects, and treatments*, Polymers, vol. 12, iss. 7, 2020, p. 1529, https://doi.org/10.3390/polym12071529.

[4] **Algarni, M., Ghazali, S.**, *Comparative study of the sensitivity of PLA, ABS, PEEK, and PETG's mechanical properties to FDM printing process parameters*, Crystals, vol. 11, iss. 8, 2021, p. 995, https://doi.org/10.3390/cryst11080995.
[5] **Jafferson, J. M., Chatterjee, D.**, *A review on polymeric materials in additive manufacturing*, Materials Today: Proceedings, vol. 46, iss. 2, 2021, pp. 1349–1365, https://doi.org/10.1016/j.matpr.2021.02.485.
[6] **Richkov, D., Rosenthal, Y., Ashkenazi, D., Stern, A.**, *Structure and fracture visualization of tilted ABS specimens processed via fused filament fabrication additive manufacturing*, Annals of "Dunarea de Jos" University of Galati. Fascicle XII, Welding Equipment and Technology, vol. 32, 2021, pp. 5–13, https://doi.org/10.35219/awet.2021.01.
[7] **Stern, A., Rosenthal, Y., Richkov, D., Gewelber, O., Ashkenazi, D.**, *Mechanical performance structure and fractography of ABS manufacturing by the fused filament fabrication additive manufacturing*, Annals of "Dunarea de Jos" University of Galati. Fascicle XII, Welding Equipment and Technology, vol. 33, 2022, pp. 5–26, https://doi.org/10.35219/awet.2022.01.
[8] **Çakan, B. G.**, *Effects of raster angle on tensile and surface roughness properties of various FDM filaments*, Journal of Mechanical Science and Technology vol. 35, iss. 8, 2021, pp. 3347–3353, https://doi.org/10.1007/s12206-021-0708-8.
[9] **Gurrala, P. K. Regalla, S. P.**, *Part strength evolution with bonding between filaments in fused deposition modelling: This paper studies how coalescence of filaments contributes to the strength of final FDM part*, Virtual and Physical Prototyping vol. 9, iss. 3, 2014, pp. 141–149, https://doi.org/10.1080/17452759.2014.913400.
[10] **Coasey, K., Hart, K. R., Wetzel, E., Edwards, D., Mackay, M. E.**, *Nonisothermal welding in fused filament fabrication*, Additive Manufacturing, vol. 33, 2020, p. 101140, https://doi.org/10.1016/j.addma.2020.101140.
[11] **Farah, S., Anderson, D. G., Langer, R.**, *Physical and mechanical properties of PLA, and their functions in widespread applications—A comprehensive review*, Advanced Drug Delivery Reviews, vol. 107, 2016, pp. 367–392, https://doi.org/10.1016/j.addr.2016.06.012.
[12] **Rajpurohit, S. R., Dave, H. K.**, *Flexural strength of fused filament fabricated (FFF) PLA parts on an open-source 3D printer*, Advances in Manufacturing, vol. 6, iss. 4, 2018, pp. 43–441, https://doi.org/10.1007/s40436-018-0237-6.
[13] **Wang, S., Ma, Y., Deng, Z., Zhang, S., Cai, J.**, *Effects of fused deposition modeling process parameters on tensile, dynamic mechanical properties of 3D printed polylactic acid materials*, Polymer Testing, vol. 86, 2020, p. 106483, https://doi.org/10.1016/j.polymertesting.2020.106483.
[14] **Algarni, M.**, *The Influence of raster angle and moisture content on the mechanical properties of PLA parts produced by fused deposition modeling*, Polymers, vol. 13, iss. 2, 2021, p. 237, https://doi.org/10.3390/polym13020237.
[15] **Kiendl, J., Gao, C.,** *Controlling toughness and strength of FDM 3D-printed PLA components through the raster layup*, Composites Part B: Engineering, vol. 180, 2020, p. 107562, https://doi.org/10.1016/j.compositesb.2019.107562.
[16] **Rajpurohit, S. R., Dave, H. K.**, *Impact strength of 3D printed PLA using open source FFF-based 3D printer*, Progress in Additive Manufacturing, vol. 6. 2021, pp. 119–131, https://doi.org/10.1007/s40964-020-00150-6.
[17] **Quanjin, M., Rejab, M. R. M., Idris, M. S., Kumar, N. M., Abdullah, M. H., Reddy, G. R.**, *Recent 3D and 4D intelligent printing technologies: A comparative review and future perspective*, *Procedia Computer Science*, vol. 167, 2020, pp. 1210–1219, https://doi.org/10.1016/j.procs.2020.03.434.
[18] **Fu, P., Li, H., Gong, J., Fan, Z., Smith, A.T., Shen, K., Khalfalla, T.O., Huang, H., Qian, X., McCutcheon, J.R., Sun, L.**, *4D printing of polymeric materials: Techniques, materials, and prospects*, *Progress in Polymer Science*, vol. 126, 2022, p.101506, https://doi.org/10.1016/j.progpolymsci.2022.101506.
[19] **Spiegel, C. A., Hackner, M., Bothe, V. P., Spatz, J. P., Blasco, E.**, *4D printing of shape memory polymers: from macro to micro*, Advanced Functional Materials, vol. 32, iss. 51, 2022, p. 2110580, https://doi.org/10.1002/adfm.202110580.
[20] **Megdich, A., Habibi, M., Laperriere, L.**, *A review on 4D printing: Material structures, stimuli and additive manufacturing techniques*, Materials Letters, vol. 337, 2023, p.133977, https://doi.org/10.1016/j.matlet.2023.133977.
[21] **Zhou, X., Ren, L., Song, Z., Li, G., Zhang, J., Li, B., Wu, Q., Li, W., Ren, L., Liu, Q.**, *Advances in 3D/4D printing of mechanical metamaterials: From manufacturing to applications*, Composites Part B: Engineering, vol. 254, 2023, p.110585, https://doi.org/10.1016/j.compositesb.2023.110585.
[22] **Zheng, Y., Huang, X., Chen, J., Wu, K., Wang, J., Zhang, X.**, *A Review of Conductive Carbon Materials for 3D Printing: Materials, Technologies, Properties, and Applications*, Materials, vol. 14, iss. 14, 2021, p. 3911, https://doi.org/10.3390/ma14143911.
[23] **Mehrpouya, M., Vahabi, H., Janbaz, S., Darafsheh, A., Mazur, T. R., Ramakrishna, S.**, *4D printing of shape memory polylactic acid (PLA)*, Polymer, vol. 230, 2021, p. 124080, https://doi.org/10.1016/j.polymer.2021.124080.
[24] **Razzaq, M.Y., Gonzalez-Gutierrez, J., Mertz, G., Ruch, D., Schmidt, D.F., Westermann, S.**, *4D printing of multicomponent shape-memory polymer formulations*, Applied Sciences, vol. 12, iss. 15, 2022, p.7880, https://doi.org/10.3390/app12157880.
[25] **Thongchom, C., Refahati, N., Roodgar Saffari, P., Roudgar Saffari, P., Niyaraki, M.N., Sirimontree, S., Keawsawasvong, S.**, *An experimental study on the effect of nanomaterials and fibers on the mechanical properties of polymer composites*, Buildings, vol. 12, iss. 1, 2022, p. 7, https://doi.org/10.3390/buildings12010007.
[26] [26] Dawoud, M., Taha, I., Ebeid, S. J., *Strain sensing behaviour of 3D printed carbon black filled ABS*, Journal of Manufacturing Processes, vol. 35, 2018, pp. 337–342, https://doi.org/10.1016/j.polymer.2021.124080.
[27] **Tirado-Garcia, I., Garcia-Gonzalez, D., Garzon-Hernandez, S., Rusinek, A., Robles, G., Martinez-Tarifa, J. M., Arias, A.**, *Conductive 3D printed PLA composites: On the interplay of mechanical, electrical and thermal behaviours*, Composite Structures, vol. 265, 2021, p.113744, https://doi.org/10.1016/j.compstruct.2021.113744.
[28] **Abdalla, A., Hamzah, H. H., Keattch, O., Covill, D., Patel, B. A.**, *Augmentation of conductive pathways in carbon black/PLA 3D-printed electrodes achieved through varying printing parameters*, Electrochimica Acta, vol. 354, 2020, p. 136618, https://doi.org/10.1016/j.electacta.2020.136618.
[29] **Beniak, J., Šooš, Ľ., Križan, P., Matúš, M., Ruprich, V.**, *Resistance and strength of conductive PLA processed by FDM additive manufacturing*, Polymers vol. 14, iss. 4, 2022, p. 678, https://doi.org/10.3390/polym14040678.
[30] **Carmona, F., Ravier, J.**, *Electrical properties and mesostructure of carbon black-filled polymers*, Carbon, vol. 40, iss. 2, 2002, pp. 151–156, https://doi.org/10.1016/S0008-6223(01)00166-X.
[31] **Balberg, I.**, *A comprehensive picture of the electrical phenomena in carbon black–polymer composites*, Carbon, vol. 40, iss. 2, 2002, pp. 139–143, https://doi.org/10.1016/S0008-6223(01)00164-6.
[32] **Király, A., Ronkay, F.**, *Temperature dependence of electrical properties in conductive polymer composites*, Polymer Testing, vol. 43, 2015, pp. 154–162, https://doi.org/10.1016/j.polymertesting.2015.03.011.
[33] **Daniel, F., Patoary, N. H., Moore, A. L., Weiss, L., Radadia, A. D.**, *Temperature-dependent electrical resistance of conductive polylactic acid filament for fused deposition modeling*, The International Journal of Advanced Manufacturing Technology, vol. 99, 2018, pp. 1215–1224, https://doi.org/10.1007/s00170-018-2490-z.
[34] **Watschke, H., Hilbig, K., Vietor, T.**, *Design and characterization of electrically conductive structures additively manufactured by material extrusion*, Applied Sciences, vol. 9, iss. 4, 2019, p. 779, https://doi.org/10.3390/app9040779.
[35] **Pentek, A., Nyitrai, M., Schiffer, A., Abraham, H., Bene, M., Molnar, E., Told, R., Maroti, P.**, The effect of printing parameters on electrical conductivity and mechanical properties of PLA and ABS based carbon composites in additive manufacturing of upper limb prosthetics, Crystals, vol. 10, iss. 5, 2020, p. 398, https://doi.org/10.3390/cryst10050398.
[36] **Stano, G., Di Nisio, A., Lanzolla, A. M., Ragolia, M., Percoco, G.**, *Fused filament fabrication of commercial conductive filaments: experimental study on the process parameters aimed at the minimization, repeatability and thermal characterization of*

electrical resistance, The International Journal of Advanced Manufacturing Technology 111, 2020, pp. 2971–2986, https://doi.org/10.1007/s00170-020-06318-2.

[37] **Namsheer, K., Rout, C.S.**, *Conducting polymers: A comprehensive review on recent advances in synthesis, properties and applications*, RSC Advances, vol. 11, iss. 10, 2021, pp. 5659–5697, https://doi.org/10.1039/D0RA07800J.

[38] **Dresler, N., Ulanov, A., Aviv, M., Ashkenazi, D., Stern, A.**, *AM-FFF of objects using commercial PLA based shape memory polymer printed by an open-source 3D printer*, Annals of "Dunarea de Jos" University of Galati. Fascicle XII, Welding Equipment and Technology, vol. 31, 2020, pp. 30–34, https://doi.org/10.35219/awet.2020.04.

[39] **Shabat, D., Rosenthal, Y., Ashkenazi, D., Stern, A.**, *Mechanical and structural characteristics of fused deposition modeling ABS material*, Annals of "Dunarea de Jos" University of Galati. Fascicle XII, Welding Equipment and Technology, vol. 28, 2017, pp. 16–24.

[40] **Solomon, A., Rosenthal, Y., Ashkenazi, D., Stern, A.**, *Structure and mechanical behavior of additive manufactured fused deposition modeling ABS*, Annals of "Dunarea de Jos" University of Galati. Fascicle XII, Welding Equipment and Technology, vol. 29, 2018, pp. 47–56. https://doi.org/10.35219/awet.2018.07.

[41] **Rosenthal, Y., Stern, A., Treivish, I., Ashkenazi, D.**, Crack propagation in flexural testing of additive manufactured acrylonitrile butadiene styrene, Annals of "Dunarea de Jos" University of Galati. Fascicle XII, Welding Equipment and Technology, vol. 30, 2019, pp. 21–26. https://doi.org/10.35219/awet.2019.03.

[42] **Gewelber. O., Rosenthal, Y., Ashkenazi, D., Stern, A.**, *Mechanical properties, structure and fracture behavior of additive manufactured FFF-ABS specimens*, Annals of "Dunarea de Jos" University of Galati. Fascicle XII, Welding Equipment and Technology, vol. 31, 2020, pp. 71–78. https://doi.org/10.35219/awet.2020.11